

Motion Selective Prediction for Video Frame Synthesis

Véronique Prinet
The Hebrew University of Jerusalem
vprinet@gmail.com

Abstract

Existing conditional video prediction approaches train a network from large databases and generalise to previously unseen data. We take the opposite stance, and introduce a model that learns from the first frames of a given video and extends its content and motion, to, e.g., double its length. To this end, we propose a dual network that can use in a flexible way both dynamic and static convolutional motion kernels, to predict future frames. The construct of our model gives us the means to efficiently analyse its functioning and interpret its output. We demonstrate experimentally the robustness of our approach on challenging videos in-the-wild and show that it is competitive w.r.t. related baselines.

1. Introduction

We consider the problem of motion prediction for future frame synthesis. While the vast majority of the recent literature in the field is dedicated to learning forecasting models from (relatively) large databases, we focus our attention on learning from few samples. Being able to learn efficiently from small data, exploiting a *good motion representation*, opens the door to a variety of new applications.

We explore for the first time predictive models that are *domain-agnostic* but *data-specific*. Our aim is to learn a model of a dynamic scene in the wild from a single video clip, and to extend/extrapolate its content and motion to, e.g., double its length. We are interested in any natural motions, such as, a bird in flight (see figure 1) or the gesture of a juggler (see the Section 6).

Learning a predictive model from a single video in the wild is challenging: 1) the generic nature of the natural motion we are seeking to model is not suitable for loss-specific or architecture-specific networks of most existing methods; 2) the choice of videos-in-the-wild implies a model capable of robust background-foreground decomposition, to be able to recover large background regions occluded by the foreground in previous frames –something that no work of our knowledge so far has demonstrated; 3) learning from a short

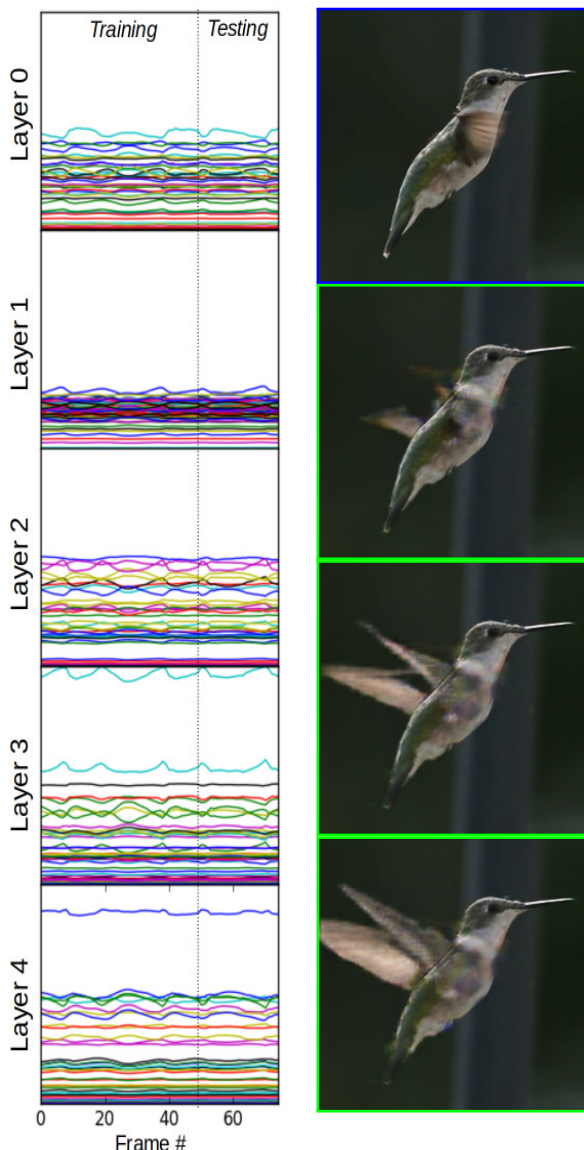


Figure 1. Conditioned on a few context frames (blue frame), the transformer, $G(\cdot)$, generates future ones (green frames). The selector modulates dynamically the amplitude of $G(\cdot)$'s motion kernels.

clip requires a quick and efficient convergence of the model at training time.

Our model is related to two different lines of work tackling the issue of motion prediction. The first one is concerned with dynamic filters, *i.e.* methods that infer input-dependent weights of a convolutional or LSTM network at each time-step, and apply these filters to a frame to predict the next one (*e.g.* [12, 5]). The second one refers to disentangled representations from unsupervised learning (*i.e.* separating the causes from the effect of an action) –approaches that usually implicitly assume simple background or semi-rigid motion [9, 16, 32].

Different from those prior works, we let our model jointly use dynamic and static elementary convolutional kernels at multi-scales. It learns in a unsupervised manner how to associate static kernels to the generation of the background image and dynamic ones to the generation of the moving foreground. Our motion representation is based on a dual network: one that learns kernels, and a second one which dynamically selects the best subset for next frame prediction. Inspired initially by the mechanism of Direction Selective (DS) cells in the retina (see [6, 29]), it is extremely simple and does not require a tailored loss or net architecture.

An other body of work related to ours is learning from few data [38, 25]. This domain is predominantly covered nowadays by the literature in meta-learning (aka, one-shot-learning). While the setting of metalearning is not ours (it relies on a large database to learn a meta-network), some of the findings are related: in particular, good initialization, or in our case, rapid exploration of distinct optimal solutions at an early stage of the training, is key to an efficient convergence of the net.

Our contributions can be summarized as follows:

1. We introduce a deep motion model for video frame prediction. To our knowledge, this is the first work which investigates learning from a single video-clip for *domain-agnostic* but *data-specific* application.
2. We show that it is possible to analyse *how* the model operates to generate the future and what it has learnt from the data.
3. We validate our approach on natural videos with cluttered background, occlusion, multiple and complex motions, and no particular semantic domain, with mid-range¹ (10-30 frames) prediction. To our knowledge, no previous work have demonstrated results on such challenging data. Our video sequences data will be made publicly available.

¹We use the term ‘mid/long range’ rather than ‘long-term’, because the difficulty of the task does not lie so much on the number of frames to generate, but rather on the amplitude of the motion between the first and the last frame.

2. Related Work

Motion representation Motion representation is a long-standing open problem in visual perception studies and computer vision [7, 22, 4, 13, 38]. Visual illusions show strong evidence that the perceived motion between consecutive images strongly depends on the image structure itself [38]. The first attempt to develop a parametric statistical model that explicitly captures the conditional dependence between the flow field and the input image structure, might be attributed to Sun *et al.* [28]. More recently, variational auto-encoders (VAE) have been shown to be an efficient means to modelling motion with learned prior [10]. Our model also learns input-dependant constraints on the flow field, albeit in a non-stochastic manner.

Video texture synthesis Dynamic texture (or textured motion) are sequences of images of moving scenes or objects that exhibit certain harmonic or stationary properties in time, often encountered in natural scenes (*e.g.*, fluid flow, clouds). Early parametric [26, 35] and non-parametric [2] approaches were mostly suitable to model global dynamic systems. Layered representations [7, 8] and deep non-linear dynamics [44, 41] were then introduced to improve the expressive power of these models. Our work took inspiration from deep non-linear auto-regressive models, in a similar fashion to [44]. However, in contrast to those cited approaches, our model can take advantage, but is not limited to, dynamic textures patterns.

Video frame prediction Recent years have sparked huge interest in conditional video prediction [12, 20, 32, 33, 24, 43, 27, 9, 10, 30, 34, 3, 39, 14, 21, 1, 19, 42, 45]. The goal is to generate future frames given a few frames history –a ‘context’. Most closely related to our work, some approaches represent motion using a set of input-dependent convolution filters, that operate on an image pyramid or at image full resolution [43, 12, 5, 34]. Amongst those, [34] is the only one of our knowledge which proposes a predictive model for domain-agnostic immediate future video frame generation. The authors use a sole adversarial loss to constrain the network, thus accounting for the uncertainty of the future. It is however restricted to short-term prediction, while we aim at exploring long-range solutions. Besides, a large body of work address the issue of disentangling video content from motion, with some applications to video synthesis [20, 32, 9, 16]. Most of those share a same basic principle: a dedicated network architecture, which hard-codes the decomposition between motion/pose and content, by the means of two distinct encoders, and the use of LSTM. In contrast, we propose a soft mechanism which simply learns how to distinguish the moving foreground from the background. This enables us, in particular, to recover occluded

background regions, something not possible from existing techniques.

Meta-learning has been applied recently by Gui *et al.* to tackle few-shot learning of human-body motion prediction [14]. Metalearning techniques are based on the principle that a base-network that is properly initialized [40, 15] (or has well-suited optimisation rules [25, 14]), as defined from a meta-learner, can be learnt –and have good generalization properties, with a few iterations of gradient descent –and a few training samples. While serving a very different goal—we do not aim at any sort of meta transfer, our model is also constructed out of two nested networks, one acting upon the other, a construct which encourages our base network to quickly reach a robust local optimum.

3. What can be learnt from few samples?

Motion domain. We are primarily interested in modelling repetitive movements (*e.g.* harmonic patterns such as waves, or state-space like motion of semi-rigid bodies such as a person walking), in static background scenes. Those motions are near deterministic. We learn by watching a single period of this movement and analyse the capacity of the model to understand symmetric motions (where only half a period is given at training).

Generalization. A conditional density model learned from scratch and from few observed frames of a given video clip is likely to memorize some aspects of the training samples –those characteristics that are common across frames. Our model is able to generalize over the motion on future frames at test time, but partly memorizes the images appearance.

Training set. When learning a model from few samples, noise can be a nuisance. Invisible stochastic noise associated to clipped pixels, over-saturated images, unstable lighting or reflective surfaces can challenge the model –it tries to learn a deterministic motion from those regions. Consequently, we prefer to process high-resolution videos (*e.g.* 256^2 pix), rather than low resolution/quality clips.

Interpretability. A good motion representation is probably a representation which enables a user to understand how the model operates. We will show that the construct of our model gives us the tool for an efficient analysis of its functioning.

4. Overview

We aim at learning an auto-regressive sequence model P_ζ , to predict $T - \delta$ future frames, given δ observed ones, $\mathbf{x}_{<\delta}$. Applying the product rule, the conditional likelihood



Figure 2. The Garden sequence. Top: generated frame; middle and bottom: foreground and ‘background’ decomposition.

over the future frames, $\mathbf{x}_{\delta:T}$, can factorized as:

$$\mathcal{L}(\zeta) = P_\zeta(\mathbf{x}_{\delta:T}|\mathbf{x}_{<\delta}) = \prod_{t'=\delta}^{T-1} P_\zeta(\mathbf{x}_{t'+1}|\tilde{\mathbf{x}}_{t'-\delta:t'}), \quad (1)$$

where the first frames of the time-series are observed, *i.e.*: $\tilde{\mathbf{x}}_{0:\delta} = \mathbf{x}_{0:\delta} = \mathbf{x}_{<\delta}$ (\mathbf{x} refers to the ground-truth image, and $\tilde{\mathbf{x}}$ is a generated one). We use a δ -order markovian assumption, *i.e.* predictions are independent conditionally of the past few frames. Future frames can be generated recursively one by one, each newly generated frame, $\tilde{\mathbf{x}}_t$, feeding the model for the next time step. The set of parameters $\zeta = \{\Phi, \theta\}$ defines the model. We learn P_ζ by minimizing the negative logarithm of equation 1, so that: $\zeta = -\arg \min_\zeta \log L(\zeta) = \arg \min_\zeta E(\zeta)$.

Our prediction model, P_ζ , is based on two nested modules: (i) a transformation model G_θ , which generates the next frame $\tilde{\mathbf{x}}_t$, by transforming the previous ones, $\mathbf{x}_{t-\delta:t}$, via a series of elementary motion kernels, $W_{\cdot,n}^l$. The size, orientation and activation amplitude of those kernels determine the transformation to be applied to the input. This encompasses both object displacement (similar to local image warping), and new pixel generation (that uncover occluded regions). (ii) a selection model, S_Φ , whose role is to choose, at each time step, which subset amongst the available motion kernels of G_θ is the most efficient to perform the desired transformation, conditioned on the input data. Specifically, the selection model outputs a probability mass function over the kernels indices of the transformation model.

This construct enables us (i) to create (*i.e.*, learn) a generic bank of specialised (elementary) directional motion kernels; (ii) to learn a mechanism by which a optimal subset of kernels can be dynamically selected and applied to a given input image, in order to generate the next one.

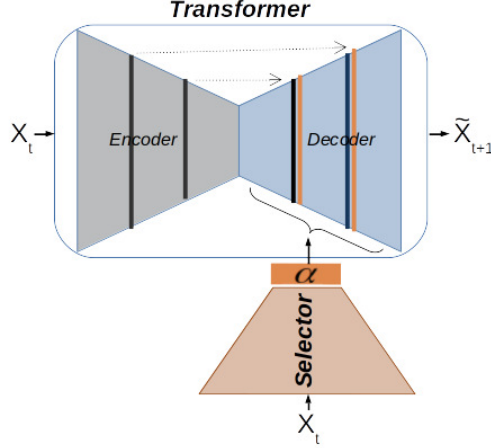


Figure 3. Our model consists of two nested networks: a transformer (top) —here represented as a 5 hidden layers encoder-decoder with skip connections, and a selector (bottom). The selector outputs weights, $\alpha(\mathbf{x})$'s, that modulate the amplitude of the transformer's decoder kernels at each layer.

As a consequence, it confers to the model some key properties: (i) flexibility at test time (because the kernel selection can adapt dynamically to each input —as in [12, 5], but through a different mechanism), (ii) robustness at training time (because the net can quickly explore very different potential solutions during the first steps of the gradient descent).

Our image transformation model can thus be written as follows:

$$\begin{aligned} \mathcal{T}_\zeta : \mathbf{x}_{t-\delta:t} &\mapsto \tilde{\mathbf{x}}_{t+1} = G_{\Phi, S_\Psi(t)}(\mathbf{x}_{t-\delta:t}) \\ &= G_\Phi(\mathbf{x}_{t-\delta:t}; S_\Psi(\mathbf{x}_{t-\delta:t})). \end{aligned} \quad (2)$$

5. Method

The transformation model and selection model (or transformer and selector respectively, for short) are nested deep networks. Following [23], we advocate for a simple network architecture. The transformer, $G_\theta : \mathbb{R}^{d \times \delta} \rightarrow \mathbb{R}^d$, is approximated by a fully convolutional encoder-decoder network with skip connection [17]: the encoder embeds the input into a small-dimensional latent variable, while the decoder transforms this latent variable, with the help of the selector, to generate the desired output image. The selector, $S_\Phi : \mathbb{R}^{d \times \delta} \rightarrow [0, 1]^{L/2 \times N}$, maps a time-dependent input onto a unit vector; L and N are respectively the transformer's total number of hidden layers and the number of channels in its encoder. The models architecture is given in figure 3.

5.1. Direction selective motion kernels

Given an input data \mathbf{x}_τ , $\tau = [t - \delta, t]$, the selector outputs a probability function over the transformer's elemen-

tary motion kernels indices. In practice, the selector will modify the behaviour of the transformer by modulating the amplitude of its kernels. The selector applies only to the transformer's decoder, and ignores the encoder.

Lets define $\hat{\alpha}(\mathbf{x}_\tau) = S_\Phi(\mathbf{x}_\tau)$ so that $\hat{\alpha} \in [0, 1]^{L/2 \times N}$ and $\int_{n=1}^N \hat{\alpha}_n^l = 1$. Then, for each building block of the decoder, the linear transformation applied to the hidden feature maps \mathcal{Y}^{l-1} at layer $l - 1 \in \{(L + 1)/2, \dots, L - 1\}$, can be defined as:

$$\alpha_n^l \leftarrow N \hat{\alpha}_n^l(\mathbf{x}_\tau)$$

$$\mathcal{Z}_{n'}^l = \sum_{n=0}^{2N-1} [\mathcal{Y}^{L-l}; \alpha^{l-1} \mathcal{Y}^{l-1}]_n * W_{n,n'}^l, \quad (3)$$

with $n' \in \{0, \dots, N - 1\}$. $[A^a; B^b]$ refers to the concatenation of feature maps A originating from the encoder at layer a of the net, via the skip-connection, with feature maps B at layer b , along the depth/channel dimension. In the above equation and the subsequent ones, we omit the bias term (which should write here $+b_n$ on the RHS), for the sake of compactness and simplicity.

Equation 3 can be developed to take a more explicit form:

$$\begin{aligned} \mathcal{Z}_{n'}^l &= \sum_{n=0}^{N-1} \mathcal{Y}_n^{L-l} * W_{n,n'}^l + \sum_{n=N}^{2N-1} \mathcal{Y}_n^{l-1} * W_{n,n'}^l \alpha_n^{l-1} \\ &= N \left(\mathbb{E}_{\mathcal{Y}_n^{L-l} \sim U()} [Q_{.,n'}^{L-l}] + \mathbb{E}_{\mathcal{Y}_n^{l-1} \sim \alpha^l} [Q_{.,n'}^l] \right) \\ &= (\mathcal{Z}_{n'}^l)^b + (\mathcal{Z}_{n'}^l)^f, \end{aligned} \quad (4)$$

where $*$ denote the convolution operation and $\mathbb{E}_{\sim \mu}[M]$ is the expected value of M given its pdf μ . In eq. 4, we set $Q_{.,n'}^{L-l} = \mathcal{Y}_n^{L-l} * W_{.,n'}^l$, and $Q_{.,n'}^l = \mathcal{Y}_n^{l-1} * W_{.,n'}^l$.

The input and time dependant behaviour of the selected kernels is encoded in the term $W_{n,n'}^l \alpha_n^{l-1} = N W_{n,n'}^l \hat{\alpha}_n^{l-1}(\mathbf{x}_\tau)$ of eq. 4, where $\hat{\alpha}^{l-1}(\mathbf{x}_\tau)$ is a scalar, and $W_{n,n'}^l \in \mathbb{R}^{f^2}$ are the weights of the $f \times f$ motion kernels.

The dynamic of the transformation being encoded in the transformer's decoder exclusively, we can expect it to be in charge of modelling the motions in the scene, *i.e.* to generate the foreground. Conversely, the encoder might be prone to simply learn (and remember) the scene background, that it transfers to the encoder via the skip connections. Figure 2 illustrates how this mechanism of foreground-background decomposition operates.

For the sake of completeness, we finally write down the expression of the very first and very last building blocks of the transformer network:

$$\mathcal{Z}_{n'}^0 = \sum_{t'=t-\delta}^t \mathbf{x}_{t'} * W_{n,n'}^0, \quad \mathcal{Y}_{n'}^0 = \rho_0(\mathcal{Z}_{n'}^0),$$

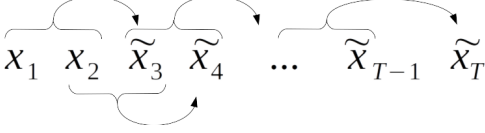


Figure 4. Schematic representation of the recursive prediction applied at training and testing time. \mathbf{x} denotes ground-truth, $\tilde{\mathbf{x}}$ are predicted images.

where $\rho(\cdot)$ is the non-linearity function, and

$$\mathcal{Z}_{n'}^L = \sum_{n=0}^{2N-1} [\mathcal{Y}^0; \alpha^L \mathcal{Y}^{L-1}]_n * W_{n,n'}^L, \quad \tilde{\mathbf{x}}_{t+1} = \rho_L(\mathcal{Z}^L).$$

We omit in this section the description of the selector, as it is similar to a classical (encoder) network. Details of the complete model architecture (number of layers, channels, non-linearity functions, *etc.*) are specified in the Supplementary material.

5.2. Loss function

We keep the loss function as simple as possible. We use the L_1 norm as reconstruction loss. In addition, we introduce a second term, a motion loss, minimizing for the total variation in the time domain:

$$\ell_{L_1}(\mathbf{x}_t) = |\tilde{\mathbf{x}}_t - \mathbf{x}_t| \quad (5)$$

$$\ell_{motion}(\mathbf{x}_t) = ||\tilde{\mathbf{x}}_t - \tilde{\mathbf{x}}_{t-1}| - |\mathbf{x}_t - \mathbf{x}_{t-1}|| \quad (6)$$

The motion loss explicitly forces the network to account for the temporal changes between consecutive frames. We investigate its effect in practice in the Results section. Hence the per-batch loss function can be written:

$$E(\zeta) = \sum_{t=t'}^{t'+K} (\ell(\mathbf{x}_t) + \mu_{motion} \mathbb{1}_{t>t'} \ell_{motion}(\mathbf{x}_t)), \quad (7)$$

where μ_{motion} is a factor weighting the two terms, $\mathbb{1}$ is the indicator function and K is the time-range prediction in the future at training time. Note that we do not impose any direct constraint on the output of the selector, $\alpha(\mathbf{x}) = S_{\Phi}(\mathbf{x})$.

5.3. Training: tips and tricks

We train the model end-to-end in a fully unsupervised manner. Similar to curriculum learning (*e.g.* [37]), we train the network with tasks of increasing difficulty. We employ training in stages:

Stage 1: Incremental K For every new batch, we randomly pick up consecutive frames in a short temporal windows $K + \delta$ from the training set, $\mathbf{x}_{t'-\delta:t'+K}$, and optimize a short form of the density, replacing T by K in equation 1. K is increased incrementally, from $K = 0$ to $K = \delta - 1$,

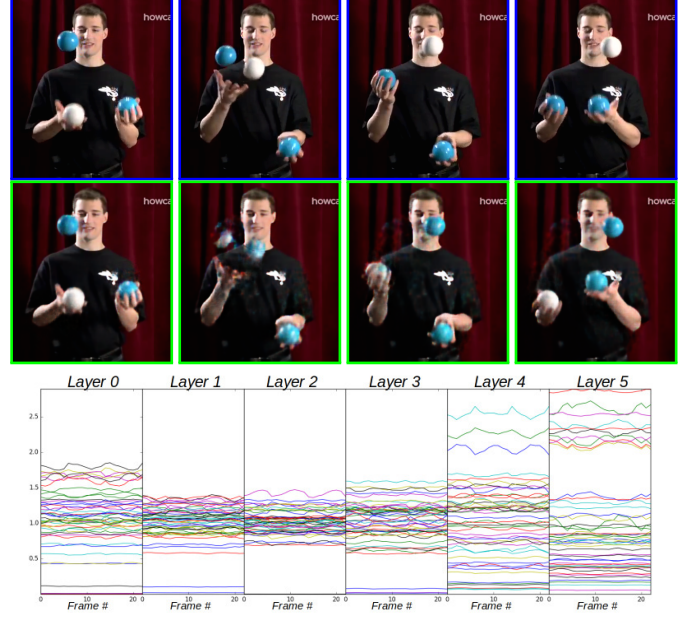


Figure 5. Failure case due to mis-”perception” of the motion periodicity. Top: Ground-truth frames. Middle: predicted frames. Note that the color of two of the balls changes from blue to white and reciprocally. Bottom: α_n^l as a function of time, for $l = [0, 5]$. The periodic pattern of the sequence is reflected in the α_n^l curves.

with a fixed number of batch iterations at each increment. Note that for $K = 0$, the model is conditioned on ground-truth frames only (*i.e.* $\tilde{\mathbf{x}} = \mathbf{x}$), for $K = 1$, a single input of the conditional set is ‘fake’ (*i.e.* generated frame), and so on until $K = \delta - 1$, where a single conditioning variable is real. We perform data augmentation by applying random left-right flips consistently among all frames of a batch.

Stage 2: Full recursive learning In this second stage, we learn to infer the whole training sequence, from the first to the last frame, following equation 1 setting $T = T_{train}$, the length of the sub-sequence available for training (typically 20-30 frames). No data augmentation is performed.

This approach is consistent with [21]. Besides, we use α as a control variable to guide the process. We survey the number of ‘active channels’, *i.e.* channels associated to a probability $\alpha_n^l > 0.5$, and adjust as necessary the setting of some of the hyperparameters (learning rate and number of channels of the transformer) so that α is not ‘sparse’ at the end of the training.

6. Experimental Results

We evaluate our approach on several challenging sequences and attempt to analyse how the network operates on specific difficult cases.



Figure 6. Failure case due to a non-deterministic motion. Top three rows: predicted (right) and associated ground-truth images (left). Lowest row: temporal average of the ground-truth and predicted sequence (18 frames). The predicted frames have captured the motion of the bird, but are too blurry.

6.1. Metrics and baselines

Following [32], we evaluate the accuracy of the reconstruction using PSNR, SSIM [36] and Mean Square measures, averaged over the length of the predicted sequence. We run and compare:

- B0 *Baseline-0*. Reference baseline, no prediction. We compute the error between the last input frame, and the next frame. This basic baseline informs us about the average motion amplitude (in terms of pixels change) between two consecutive frames.
- B1 *Baseline-1*. Encoder-encoder. The sole transformation model $G_\theta()$ is trained, the selection model is inactive; we set $\mu_{motion} = 0$.
- M1 *DN w/o motion loss*. Our dual net model — $G_\theta()$ and $S()_\Phi$ are trained jointly; we set $\mu_{motion} = 0$.
- M2 *FDN*. Our dual net model, trained with motion loss. We set $\mu_{motion} = 10$, unless specified otherwise.

6.2. Data and results

Bird. The complexity of the motion of the bird flapping wings, and the subtle change of the foreground texture (semi-transparency of the wings due to the fast motion) makes the sequence challenging (figure 11). The sequence was downloaded from Youtube, cropped and resized to 256×256 pixels. It comprises 80 frames, 50 of which being used for training. Motion is learned with a conditioning of four frames. For testing, we input to the net four frames that it has not seen at training, and predict future 25 frames. Figure 11 shows that our approach synthesises correctly motion and appearance, while the baseline tends to introduce color artefact.

In order to test whether the network just remembers the whole sequence or adopts a smarter behaviour, we also evaluate the prediction result obtained from a different conditioning/entry-point (illustrations are given in the Supplementary Material). Indeed, we can show that the model ‘reads’ correctly the given inputs and forecasts properly the next frames/poses. It suggests that, while probably the net keeps in memory some of the pose information of the bird wings, it understands the rule of transformation from one frame/pose to the next one.

We show in figure 1 the α values inferred by the trained selector $S()$ as a function of time (frame #). Each curve characterizes the variation of the amplitude of a given motion kernel at each layer of the transformer’s decoder. To generate this figure, we gave the net the first frames of the sequence, and let it predict the entire video. The last 30 frames had not been seen by the net during training. One can observe that the α -curves reflects a periodic pattern, consistent with the bird motion. The α -curves represent the visual motion pattern in a non-trivial way.

Boy on a bicycle. This example shows a sequence with cluttered textured background (figure 8). The dominant motion is mainly translational, with a rotational movement of the legs added to it. The sequence was acquired by a Canon EOS camera, with a resolution of 1280, cropped then resized to 100×320 pix. It comprises 57 frames, 30 of which being used for training. Motion is learned with a conditioning of three frames. To illustrate the results, we feed the net with three frames of the sequence unseen at training time, and predict future frames until the boy leaves the camera’s field of view. Results and comparison with baselines are shown in figure 8. While all three approaches model correctly the translational motion, the baselines either introduce some foreground color change (B1) or lose foreground details and shape contours.

In order to analyse how operated the reconstruction and foreground-background separation, we synthesise a frame by setting $(Z_{n'}^L)^b = 0$ for foreground generation, and $(Z_{n'}^L)^f = 0$ for background generation, in equation 4. Results are illustrated in figure 2. The foreground image de-



Figure 7. Bird sequence. Top (blue frames): input conditioning (left) and six frames (three first and three last frames, out of 25) ground-truth (that the model has not seen at training). Yellow frames: prediction results from B1. Orange frames: M1. Green frames: M2 (our FDN). Gray frames: L_2 error between ground-truth and our full model (FDN) prediction.

picts the boy on its bicycle; it also contains a ‘phantom’ of the bike seen in the previous frame (it appears like a shadow). The ground floor has been mistaken by an object in motion, probably due to its high surface reflectivity. The α -curves of this sequence are constant over time, in agreement with the uniform bike’s motion (see Supp. Material).

Ocean. We selected a sequence from the YUP++ dataset [11] depicting ocean waves and a boat moving (static camera # 28, Ocean category), that we cropped to 200^2 pix and down-sampled in the time domain, to eventually get a sequence of 50 frames. The boat displacement is uniform, while the waves are characterized by harmonic oscillations. The colors are tern, without good contrast between the boat’s hull and the sea. We learn the model from 20 frames, using three frames for conditioning. We predict over the next 26 frames. Results are illustrated in figure 8. The motion loss, accounted for only in our full model (green frames), makes here a crucial difference and allows our model to distinguish correctly the sea from the boat’s hull.

6.3. Failure cases

We illustrate briefly two failure cases, the Juggler (fig. 5) and the Bird#2 (fig. 6). In the first case, the model understands the motion but mis-interprets its periodicity: it does not differentiate between the blue and white balls, as it should. The α -curves of this sequence suggests that the

	B0	B1	M1	M2 (FDN)
Bird	22.2	23.1/0.913	23.6/0.922	24.2/0.923
Garden	19.5	20.3/0.682	20.5/0.70	20.42/0.695
Ocean	25.6	26.1/0.943	27.06/ 0.963	27.7 /0.955

Table 1. Quantitative analysis (average PSNR/SSIM over the predicted sequence length), for the Bird, Garden and Ocean clips.

model builds an internal representation of the video which is invariant to the balls’ color.

The Bird#2 case shows a limitation of the model: it does not account for the uncertainty of the future —the motion of the bird feeding its nestling is repetitive but with high variance.

7. Conclusion

We have introduced a model for future frame synthesis from a single video-clip in-the-wild. Inspired initially by the mechanism of Direction Selective cells in the retina, our motion representation is based on a dual network: one that learns kernels, and a second one which dynamically selects the best subset for next frame prediction. Our frame generations compare favourably with baseline approaches on challenging videos. As future work, we plan to investigate the potential of such a dual-net construct on other tasks, *e.g.* motion composition, or motion transfer. An other direction would be to extract a richer latent motion representation.

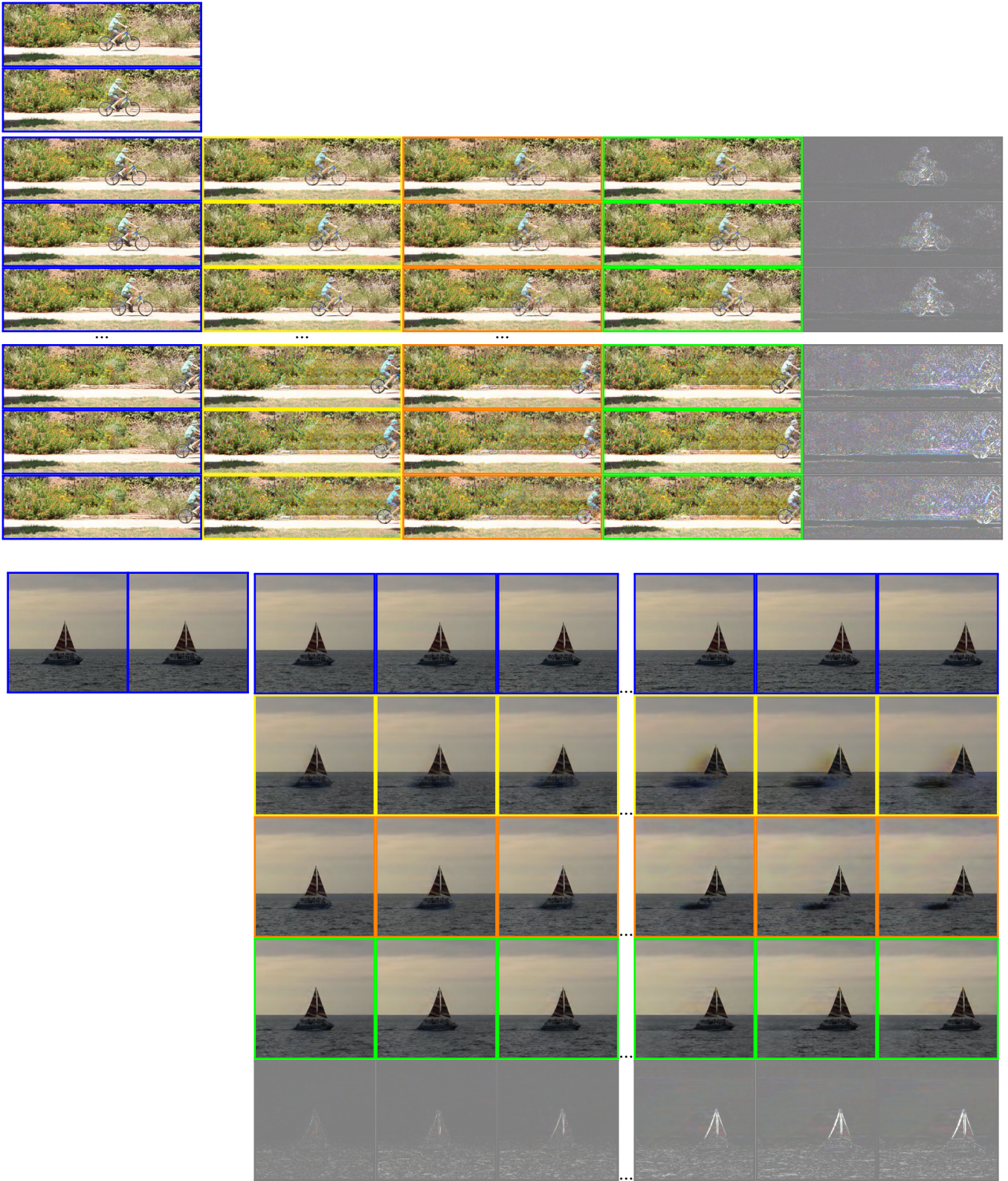


Figure 8. Garden (top) and Ocean (bottom) sequences. Conditioning and ground-truth (blue frames), predictions results from Baseline-1 (yellow), our DN w/o motion loss (M1, orange), and our FDN (M2, green) and associated L_2 error (gray). (see caption of Fig. 11)

Acknowledgment

We would like to acknowledge Michael Werman and Shmuel Peleg for helpful discussions, constructive feedback and suggestions during this project.

References

- [1] M. Babaeizadeh, C. Finn, D. Erhan, R. Campbell, and S. Levine. Stochastic variational video prediction. In *ICLR*, 2018.
- [2] Z. Bar-Joseph, R. El-Yaniv, D. Lischinski, and M. Werman. Texture mixing and texture movie synthesis using statistical learning. *IEEE Transactions on Visualization and Computer Graphics archive*, 7(2):120–135, 2002.
- [3] P. Bhattacharjee and S. Das. Temporal coherency based criteria for predicting video frames using deep multi-stage generative adversarial networks. In *NIPS*, 2017.
- [4] M. Black and P. Anandan. The robust estimation of multiple motions: Parametric and piecewise-smooth flow fields. *Computer Vision and Image Understanding*, 63, 1996.
- [5] B. D. Brabandere, X. Jia, T. Tuytelaars, and L. V. Gool. Dynamic filter networks. In *NIPS*, 2016.
- [6] K. L. Briggman, M. Helmstaedter, and W. Denk. Wiring specificity in the direction-selectivity circuit of the retina. *Nature*, 471:183–188, March 2011.
- [7] A. Chan and N. Vasconcelos. Layered dynamic texture. *IEEE Transactions on Pattern Analysis and Machine Intelligence (PAMI)*, 2009.
- [8] Y. Chuang, D. Goldman, K. Zheng, B. Curless, D. Salesin, and R. Szeliski. Animating pictures with stochastic motion texture. *ACM Transactions on Graphics*, 2005.
- [9] E. Denton and V. Birodkar. Unsupervised learning of disentangled representations from video. In *NIPS*, 2017.
- [10] E. Denton and R. Fergus. Stochastic video generation with a learned prior. In *ICML*, 2018.
- [11] K. Derpanis, M. Lecce, K. Daniilidis, and R. Wildes. Dynamic scene understanding: The role of orientation features in space and time in scene classification. In *CVPR*, 2012.
- [12] C. Finn, I. Goodfellow, and S. Levine. Unsupervised learning for physical interaction through video prediction. In *NIPS*, 2016.
- [13] D. Fleet. Design and use of linear models for image motion analysis. *International Journal of Computer Vision*, 36, 2000.
- [14] L. Gui, Y. Wang, D. Ramanan, and J. Moura. Few-shot human motion prediction via meta-learning. In *ECCV*, 2018.
- [15] D. Ha, A. Dai, and Q. V. Le. Hypernetworks. In *ICLR*, 2016.
- [16] J. Hsieh, B. Liu, D. Huang, L. Fei-Fei, and J.-C. Niebles. Learning to decompose and disentangle representations for video prediction. <https://arxiv.org/abs/1806.04166>, 2018.
- [17] P. Isola, J.-Y. Zhu, J. Zhou, and A. Efros. Image-to-image translation with conditional adversarial nets. In *CVPR*, 2017.
- [18] D. P. Kingma and J. Ba. Adam: a method for stochastic optimization. <https://arxiv.org/abs/1412.6980>, 2017.
- [19] A. Lee, R. Zhang, F. Ebert, P. Abbeel, C. Finn, and S. Levine. Stochastic adversarial video prediction. <https://arxiv.org/abs/1804.01523v1>.
- [20] W. Lotter, G. Kreiman, and D. Cox. Deep predictive coding networks for video prediction and unsupervised learning. In *ICLR*, 2017.
- [21] C. Lu, M. Hirsh, and B. Scholkopf. Flexible spatio-temporal network for video prediction. In *CVPR*, 2017.
- [22] B. D. Lucas and T. Kanade. An iterative image registration technique with an application to stereo vision. In *Imaging Understanding Workshop*, 1981.
- [23] J. Martinez, M. Black, and J. Romero. On human motion prediction using recurrent neural networks. In *CVPR*, 2017.
- [24] M. Mathieu, C. Couprie, and Y. LeCun. Deep multiscale video prediction beyond mean square error. In *ICLR*, 2016.
- [25] A. Rusu, D. Rao, J. Sygnowski, O. Vinyals, R. Pascanu, S. Osindero, and R. Hadse. Meta-learning with latent embedding optimisation. <https://arxiv.org/abs/1807.05980>, 2018.
- [26] S. Soatto, G. Doretto, and Y. Wu. Dynamic textures. In *ECCV*, 2001.
- [27] N. Srivastava, E. Mansimov, and R. Salakhutdinov. Unsupervised learning of video representations using lstms. In *ICML*, 2015.
- [28] D. Sun, S. Roth, J. Lewis, and M. Black. Learning optical flow. In *ECCV*, 2008.
- [29] W. Sun, Q. Deng, W. Levick, and S. He. On direction-selective ganglion cells in the mouse retina. *The Journal of Physiology*, pages 197–202, 2006.
- [30] S. Tulyakov, M. Liu, X. Yang, and J. Kautz. Mocogan: Decomposing motion and content for video generation. In *CVPR*, 2018.
- [31] D. Ulyanov, A. Vedaldi, and V. Lempitsky. Deep image prior. <https://arxiv.org/abs/1711.10925>, 2017.
- [32] R. Villegas, J. Yang, S. Hong, X. Lin, and H. Lee. Decomposing motion and content for natural video sequence prediction. In *ICLR*, 2017.
- [33] R. Villegas, J. Yang, Y. Zou, S. Sohn, X. Lin, and H. Lee. Learning to generate long-term future via hierarchical prediction. In *ICML*, 2017.
- [34] C. Vondrick and A. Torralba. Generating the future with adversarial transformers. In *CVPR*, 2017.
- [35] Q. Wang and S. Zhu. Modeling textured motion: particle, wave and sketch. In *ICCV*, 2003.
- [36] Z. Wang, A. Bovik, H. Sheikh, and E. Simoncelli. Image quality assessment: from error visibility to structural similarity. *IEEE Transactions on Image Processing*, 2004.
- [37] D. Weinshall, G. Cohen, and D. Amir. Curriculum learning by transfer learning: Theory and experiments with deep networks. In *ICML*, 2018.
- [38] Y. Weiss, E. Simoncelli, and E. Adelson. Motion illusions as optimal percepts. *Nature Neuroscience*, 5(6):598–604, June 2002.
- [39] N. Wichers, R. Villegas, D. Erhan, and H. Lee. Hierarchical long-term video prediction without supervision. In *ICML*, 2018.

- [40] T. Wu, J. Peurifoy, I. Chuang, and M. Tegmark. Meta-learning autoencoders for few-shot prediction. <https://arxiv.org/abs/1807.09912>, 2018.
- [41] J. Xie, S. Zhu, and Y. Wu. Synthetising dynamic patterns by spatial temporal generative conv net. In *CVPR*, 2017.
- [42] J. Xu, B. Ni, Z. Li, S. Cheng, and X. Yang. Structure preserving video prediction. In *cvpr*, 2018.
- [43] T. Xue, J. Wu, K. L. Bouman, and W. T. Freeman. Visual dynamics: Probabilistic future frame synthesis via cross convolutional network. In *NIPS*, 2016.
- [44] X. Yan, H. Chang, A. Shan, and X. Chen. Modeling video dynamics with deep dynencoder. In *ECCV*, 2014.
- [45] T. Yu, L. Wang, H. Gu, S. Xiang, and C. Pan. Deep generative video prediction. *Pattern Recognition Letters*.

Appendices

We provide additional information regarding:

1. Specific architecture and hyper-parameters of the model;
2. Detailed quantitative results of the *Bird*, *Garden* and *Ocean* clips, that supplement the results’ summary given in the main article.
3. Additional qualitative results.

A. Network architecture and hyper-parameters

Preprocessing The input frames are normalised (*i.e.* scaled by a factor of 255) and centralized to $[-1, 1]$.

Transformation model. The input tensor to the transformation model is of size $[C, H, W, T]$, where $C = \{1, 3\}$ is the number of color channels, H and W are the dimensions of the frames, and $T = \delta$ it the length of the conditioning (typically three to four frames). The output tensor is of size $[C, H, W, 1]$.

The net architecture is based on a U-net, as defined in [17]. Each building block of the encoder and of the decoder is defined as: RELU - (DE)CONV - INSTANCENORM, except the first and the last layer. The first one comprises a sole CONV, and the last one substitutes the instance normalisation [31] with a TANH() non linearity. The CONV operation (resp. DECONV) is performed with a stride of two (resp. upscaling of two). Different from [17], the number of channels (*i.e.* the network width) of the hidden layers is constant across layers and fixed to N . The convolutional filters size, f_t , is set to 4×4 .

The width N and the depth L (*i.e.* number of hidden layers) are set manually for each video. N is set according to the complexity of the background to model (more channels for more complex videos). L is set so that the hidden feature layer of smallest spatial dimension (*i.e.* at layer $L/2$) has a dimension of at least three pixels, at most seven.

Selection model. A first layer of the selection model transforms the input \mathbf{x}_τ into difference images: it computes the absolute temporal difference between consecutive

	N	L	ndf	frame size
Bird	50	12	16	256×256
Garden	80	10	16	100×320
Ocean	50	12	16	200×200
Juggler	50	14	16	340×300
Cat	30	10	16	305×320

Table 2. Hyper-parameter setting.

frames. This process allows to discard the scene static background.

The main architecture of the selector net is again borrowed from [17]’ encoder. It takes as input a tensor of size $[C, H, W, T - 1]$. It has a RELU - CONV - BATCHNORM structure at each building block (except the first ones which both ignore the normalisation), with a stride of two, and a doubling number of channels from one layer to an other. The last layer is a fully connected one. The output vector is reshaped to a matrix $N \times L/2$. The columns of the matrix are normalised with a SOFTMAX() function (so that $\sum_n \alpha_n^l = 1$). The number of hidden layers is set to $L/2$. The channels number at the first layer, ndf , is a free parameter. The convolutional filters size, f_s , is set to 5×5 .

In addition, we may add, before the fully connected layer, convolutional blocks, that leave unchanged the spatial dimension of the hidden layers (*i.e.* stride one), but reduce the number of channels (divided by two at each new block). These extra blocks are meant to reduce the size of the fully connected layer, so that the two networks (selector and transformer) are of similar capacity (same order of magnitude).

Learning We learn the model using Adam optimizer [18] (beta value set to 0.9), and a initial learning rate set to either $1.e^{-3}$ or $2.e^{-4}$. The selector and the transformer weights are updated at each iteration. The learning rate decreases by a factor of two every 2K iterations. We proceed with early stopping in stage-2 of the training procedure (Section 5.3).

B. Detailed quantitative results

Figure 9 summarizes the quantitative comparison among: i) our Full Dual net, ii) a variation of our Dual net —trained with a sole ℓ_{L_1} loss, setting $\mu_{motion} = 0$ —, and iii) a baseline —defined by an auto-encoder, trained similarly with $\mu_{motion} = 0$. For our full model (full DN), the value of μ_{motion} is set to 10, except for the Ocean sequence (for which it is 1).

We investigate the effect of the prediction range (*i.e.* time steps into the future) on the results accuracy, using PSNR, SSIM [36], L_2 -norm as metrics. Our Full Dual model outperforms the two other methods, based on the MSE and PSNR metrics, on the scenes with complex motion (*i.e.* the Bird and the Ocean). As expected the error increases with the time range, for the Garden and Ocean clips: the error accumulates as the foreground object (the bicycle or the boat) moves away from its original position. However, the pattern of the Bird sequence is quite different (only the wings of the bird are animated, there is no global motion). Interestingly, it suggests that the net remembers the poses of the wings (some better than other) but learn and infer the sequence of these poses.

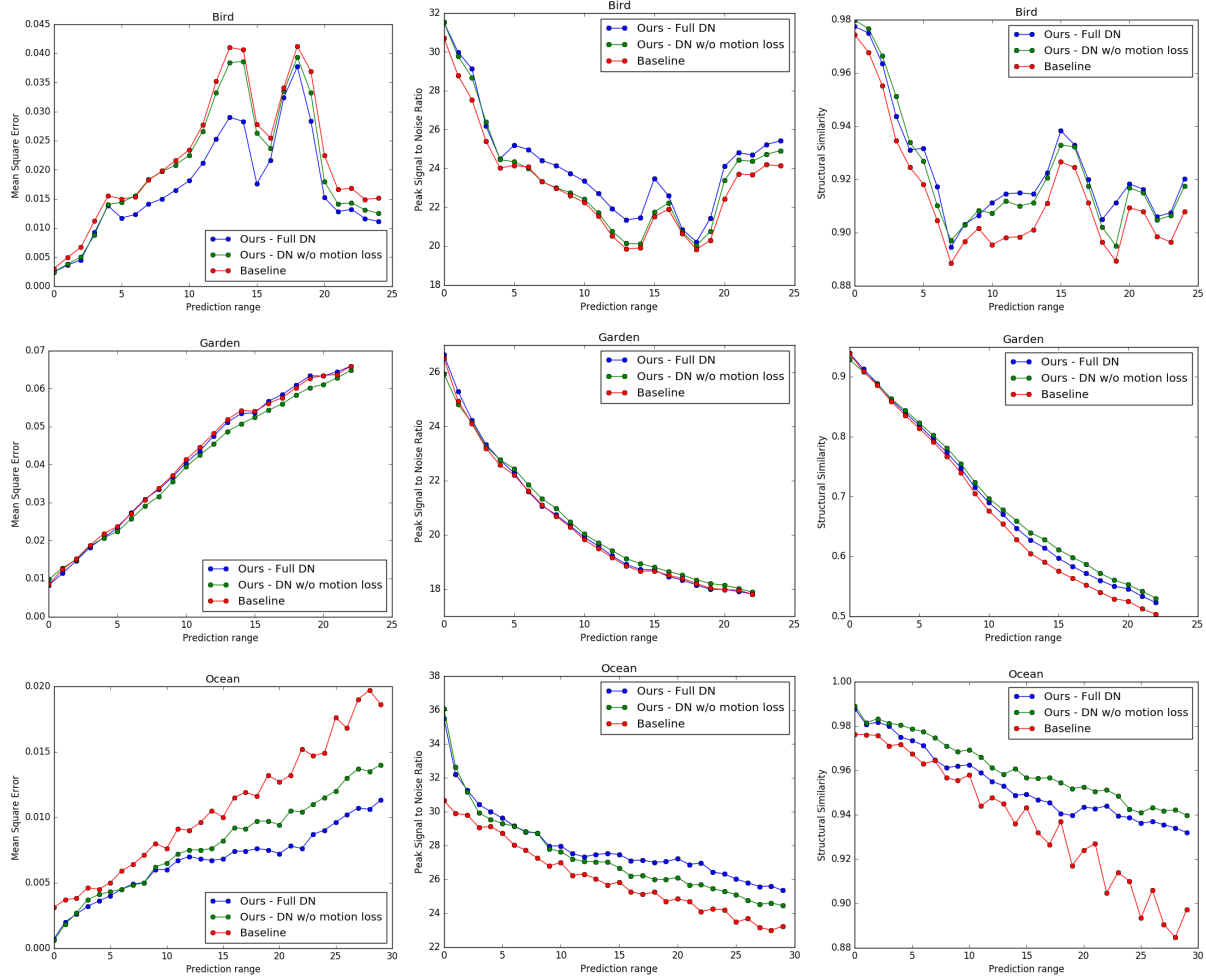


Figure 9. Quantitative comparison between our model (Dual Net) with and without motion loss and the baseline. The model is given a few context frames, and predicts the rest of the sequence recursively, one frame at a time.

C. Additional results

Cat sequence

The Cat sequence (figure 10) was downloaded from Youtube, and subsampled in time and space by a factor of 2. It comprises 32 frames (105×320 pixels). The motion reflects the global translational displacement and the local movement of the cat's legs. To illustrate the results, we feed the net with three frames that have been seen during training (no 25 and onward), and predict over thirty frames (with no ground truth available for most of the predicted sequence). The visual comparison of our FDN results (green frames, figure 10) shows sharper contour and better motion forecast from our model, in comparison to the baselines (B1, M1).

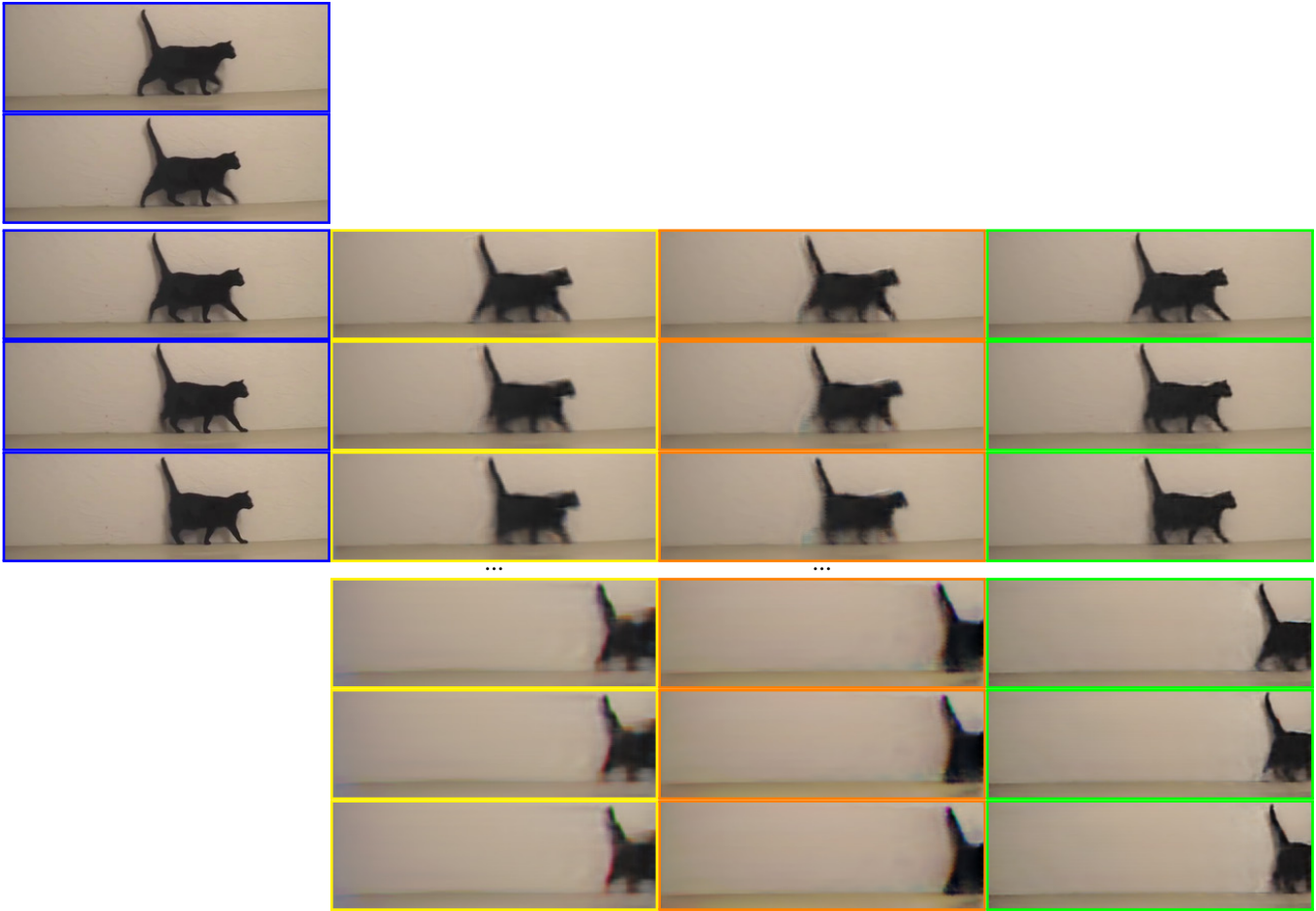


Figure 10. Cat sequence. Conditioning and ground-truth (blue frames), predictions results from Baseline-1 (yellow), our DN w/o motion loss (M1, orange), and our FDN (M2, green)



Figure 11. Bird sequence. Two different input conditionings (left, blue frames) and consecutive six frames prediction from our Full Model (Green frames). Blue frames (right) correspond to ground truth.